Acta Crystallographica Section B
Structural Science
ISSN 0108-7681

Structural phase transitions, and Br···N and Br···Br interactions in 1-phenyl-2-methyl-4-nitro-5-bromoimidazole

Maciej Kubicki

Faculty of Chemistry, Adam Mickiewicz University, Grunwaldzka 6, 60-780 Poznań, Poland

Correspondence e-mail: mkubicki@amu.edu.pl

Received 3 December 2003
Accepted 12 March 2004

Crystals of $C_{10}H_8N_3O_2Br$ undergo two reversible phase transitions between 295 and 100 K. The first, of an order–disorder nature, is a second-order transition and takes place continuously over a wide temperature range. This transition is connected with the doubling of the length of the *c* axis of the unit cell and with the change of the space group from $P2_1/m$ with $Z' = 1/2$ (room-temperature α-phase) to $P2_1/c$, $Z' = 1$ (β-phase, 200–120 K). During this transition the molecule loses the C_s symmetry of the α-phase. The second transition takes place between 118 and 115 K, and is accompanied by a change of the crystal symmetry to the triclinic space group $P\bar{1}$ (low-temperature γ-phase). This second phase transition is accompanied by the twinning of the crystal. Neither the molecular geometry nor the crystal packing shows any dramatic changes during these phase transitions. Halogen bonds C—Br···N and dihalogen interactions Br···Br play a crucial role in determining the crystal packing and compete successfully with other kinds of weak intermolecular interactions.

1. Introduction

4-Nitroimidazole derivatives have been successfully used for studying weak intermolecular interactions. For example, the crucial role of C—H···O and C—H···N hydrogen bonds in the crystal structure of 1-phenyl-4-nitroimidazole has been determined both by the analysis of the packing modes (Kubicki *et al.*, 2001) and by the topological analysis of the experimental charge density distribution (Kubicki *et al.*, 2002). Similar interactions determine the crystal structures of 1-phenyl-2-methyl-4-nitroimidazole (Kowalski, 1995) and 1-phenyl-2-methyl-4-nitro-5-methoxyimidazole (Kubicki, 2004). It therefore seemed interesting to study the crystal structure of a closely related compound, 1-phenyl-2-methyl-4-nitro-5-bromoimidazole [(1), see (I) below], that has similar possibilities for making weak hydrogen bonds. This compound offered the possibility of comparing the relative importance of weak hydrogen bonds and the so-called *halogen bonds*, *i.e.* the attractive interactions between the carbon-bound halogen atom and atoms that have lone pairs (*e.g.* Hassel & Rømming, 1962; Bent, 1968; Dahl & Hassel, 1970, 1971; Hassel, 1970; for the recent reviews see, for example, Legon, 1999; Metrangolo & Resnati, 2001; Metrangolo *et al.*, 2003). Also, the interactions between halogen atoms (that can be termed *dihalogen bonds*), leading to the $X\cdots X$ contacts much shorter than the sums of their van der Waals radii, have been recognized for a long time (*e.g.* Rossmann & Lipscomb, 1958; Wunderlich & Lipscomb, 1960; Sakurai *et al.*, 1963) and these interactions can also be expected in the crystal structure of (1).

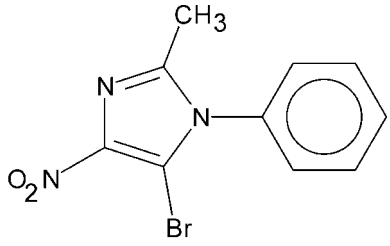

(I)

Quite unexpectedly, the analysis of the crystal structure of (1) at different temperatures has shown two different reversible structural phase transitions between room temperature and 90 K. The first is of an order–disorder nature and is connected with the loss of the internal symmetry C_s of the molecule, while the second one changes the crystal point group of symmetry from C_{2h} to C_i and is accompanied by the twinning of the crystal. According to the thermodynamical classification of phase transitions (for detailed discussion and references see Herbstein, 1996) the first transition is probably of second order, while the second is first order.

2. Experimental

The crystals of the title compound were kindly provided by Dr Paweł Wagner from Silesian University of Technology, Gliwice, Poland (presently at Massey University, Palmerton North, New Zealand; the synthetic procedure will be published elsewhere). Nice, prismatic crystals, appropriate for data collection, were obtained by a slow evaporation from a methanol solution.

Data collections were performed with an Oxford Diffraction KM4CCD four-circle diffractometer equipped with a CCD detector (Oxford Diffraction, 2003*a*), using graphite-monochromated Mo $K\alpha$ radiation (λ = 0.71073 Å). Diffraction data were collected at seven different temperatures: 295, 250, 200, 170, 150, 120 and 100 K. In each case the temperature was controlled with an Oxford Cryosystems cooling device; the stability was estimated as ±0.5 K. Two different crystals were used: the first set of measurements was carried out at 295, 120 and 100 K. Data collection was performed at every temperature in eight runs with different diffractometer angle settings. As these data showed that there are phase transitions, a second crystal was used for another set of measurements at 250, 200, 170 and 150 K.[1] These data collections were performed more rapidly, with four runs (only at 200 K was the measurement performed again in eight runs). Additionally, for some different temperatures in the range 140–100 K nine short data collections (around 100 frames each) were carried out in order to obtain estimates for the unit-cell parameters.

For each of the datasets the unit-cell parameters were calculated by the least-squares fitting of the setting angles of the strongest reflections taken from the whole set of measurements. Further analysis showed that for all datasets at $T \geq 120$ K there are two possibilities for the unit cell, one of these cells being twice as large as the other ($l' = 2l$; see §3). Therefore, in these cases the data corrections for full datasets were carried out in both of the possible unit cells. Data were corrected for Lorentz and polarization effects (Oxford Diffraction, 2003*b*), and then corrected for absorption and merged by *Sortav* (Blessing, 1989).

For every set of data in the range 295–120 K the structure solutions and refinements were performed for three models: $P2_1/m$ with $Z' = 1/2$, $P2_1$ with $Z' = 1$, and $P2_1/c$ with $Z' = 1$ and a unit cell twice as long along **c**. *SIR*2002 (Burla *et al.*, 2003) was able to find the structure solution for every model at every temperature. The refinements were carried out by full-matrix least-squares with *SHELXL*97 (Sheldrick, 1997) without any constraints, in order to have the clear comparison of different models. If deemed applicable, extinction corrections were applied.

At 100 K the crystals became twins; the structure was solved, but it could not initially be refined below R_1 = 0.18. Analysis of the reciprocal lattice (Fig. 1) showed that the reflections should be divided into three groups according to the k index:

(i) $|k|$ = 2, 3, 4, 8, 9: the spots from the two twinned fragments are well resolved and therefore they did not need special treatment.

(ii) $|k|$ = 0, 6: the spots overlap: for these reflections the BASF and TWIN commands (Sheldrick, 1997) were applied (HKLF 5 with batch numbers 1 and −2).

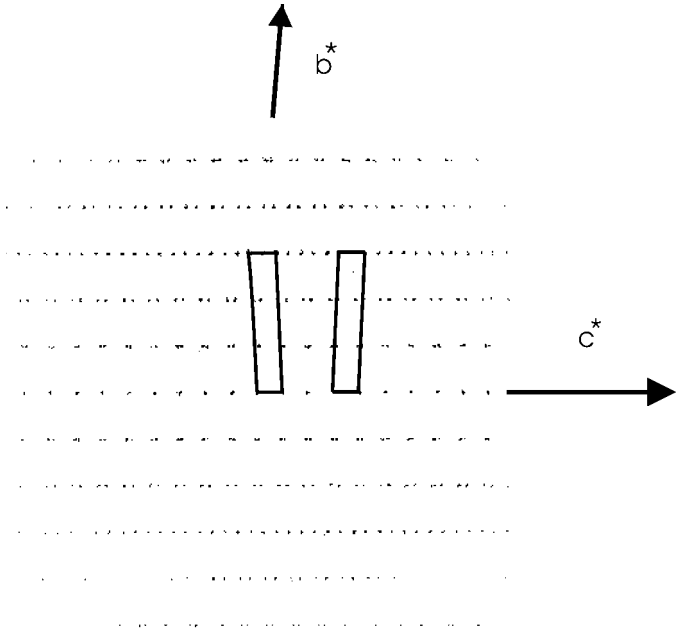

Figure 1
Representation of the 100 section of reciprocal space at 100 K showing the apparent effects of twinning. Two possible unit cells (for clarity, the boxes contain three unit cells) related by a mirror plane are drawn.

[1] Supplementary data for this paper are available from the IUCr electronic archives (Reference: BK5005). Services for accessing these data are described at the back of the journal.

Table 1
Experimental details.

Details for all refinements (including those at 170 and 150 K) are given in the CIF, which has been deposited.

	295 K	250 K	200 K	120 K	100 K
Crystal data					
Chemical formula	$C_{10}H_8BrN_3O_2$	$C_{10}H_8BrN_3O_2$	$C_{10}H_8BrN_3O_2$	$C_{10}H_8BrN_3O_2$	$C_{10}H_8BrN_3O_2$
M_r	282.10	282.10	282.10	282.10	282.10
Cell setting, space group	Monoclinic, $P2_1/m$	Monoclinic, $P2_1/m$	Monoclinic, $P2_1/c$	Monoclinic, $P2_1/c$	Triclinic, $P\bar{1}$
a, b, c (Å)	7.0281 (10), 6.9388 (9), 11.5612 (15)	7.0180 (14), 6.9160 (12), 11.546 (2)	6.9955 (9), 6.8657 (8), 22.990 (2)	6.9723 (5), 6.8169 (4), 22.9000 (12)	6.9654 (10), 6.8215 (10), 11.3983 (17)
α, β, γ (°)	90, 106.735 (12), 90	90, 106.410 (15), 90	90, 106.356 (10), 90	90.00, 106.478 (6), 90.00	92.683 (13), 106.506 (12), 90.277 (12)
V (Å^3)	539.92 (13)	537.57 (17)	1059.5 (2)	1043.72 (11)	518.60 (14)
Z	2	2	4	4	2
D_x (Mg m^{-3})	1.735	1.743	1.769	1.795	1.806
Radiation type	Mo $K\alpha$	Mo $K\alpha$	Mo $K\alpha$	Mo $K\alpha$	Mo $K\alpha$
No. of reflections for cell parameters	4253	668	2101	3121	1221
θ range (°)	3–20	3–20	3–22	3–20	4–22
μ (mm^{-1})	3.80	3.81	3.87	3.93	3.95
Temperature (K)	295 (1)	250 (1)	200 (1)	120 (1)	100 (1)
Crystal form, colour	Prism, colourless	Prism, colourless	Prism, colourless	Prism, colourless	Prism, colourless
Crystal size (mm)	0.3 × 0.25 × 0.1	0.5 × 0.3 × 0.1	0.5 × 0.3 × 0.1	0.3 × 0.25 × 0.1	0.5 × 0.3 × 0.1
Data collection					
Diffractometer	KUMA KM4CCD four-circle	KUMA KM4CCD four-circle	KUMA KM4CCD four-circle	KUMA KM4CCD four-circle	KUMA KM4CCD four-circle
Data collection method	ω-scan	ω-scan	ω-scan	ω-scan	ω-scan
Absorption correction	Multi-scan (based on symmetry-related measurements)	Multi-scan (based on symmetry-related measurements)	Multi-scan (based on symmetry-related measurements)	Multi-scan (based on symmetry-related measurements)	Multi-scan (based on symmetry-related measurements)
T_{min}	0.382	0.326	0.355	0.378	0.305
T_{max}	0.696	0.673	0.725	0.573	0.594
No. of measured, independent and observed reflections	5105, 1521, 1342	3360, 1473, 1097	13 871, 2719, 1610	13 861, 2788, 2349	6344, 1720, 1586
Criterion for observed reflections	$I > 2\sigma(I)$	$I > 2\sigma(I)$	$I > 2\sigma(I)$	$I > 2\sigma(I)$	$I > 2\sigma(I)$
R_{int}	0.042	0.054	0.061	0.045	0.072
θ_{max} (°)	29.7	29.6	29.4	29.8	29.9
Range of h, k, l	$-9 \Rightarrow h \Rightarrow 9$ $-9 \Rightarrow k \Rightarrow 9$ $-6 \Rightarrow l \Rightarrow 15$	$-6 \Rightarrow h \Rightarrow 9$ $-9 \Rightarrow k \Rightarrow 9$ $-15 \Rightarrow l \Rightarrow 15$	$-9 \Rightarrow h \Rightarrow 9$ $0 \Rightarrow k \Rightarrow 9$ $0 \Rightarrow l \Rightarrow 30$	$-7 \Rightarrow h \Rightarrow 9$ $-7 \Rightarrow k \Rightarrow 9$ $-31 \Rightarrow l \Rightarrow 30$	$-9 \Rightarrow h \Rightarrow 9$ $-9 \Rightarrow k \Rightarrow 9$ $-15 \Rightarrow l \Rightarrow 15$
Refinement					
Refinement on	F^2	F^2	F^2	F^2	F^2
$R[F^2 > 2\sigma(F^2)]$, $wR(F^2)$, S	0.029, 0.075, 1.02	0.042, 0.100, 1.00	0.049, 0.137, 1.13	0.033, 0.068, 1.07	0.058, 0.161, 1.11
No. of reflections	1521	1473	2719	2788	1720
No. of parameters	93	91	148	178	146
H-atom treatment	Mixture of independent and constrained refinement	Mixture of independent and constrained refinement	Mixture of independent and constrained refinement	Refined independently	Mixture of independent and constrained refinement
Weighting scheme	$w = 1/[\sigma^2(F_o^2) + (0.0509P)^2]$, where $P = (F_o^2 + 2F_c^2)/3$	$w = 1/[\sigma^2(F_o^2) + (0.047P)^2]$, where $P = (F_o^2 + 2F_c^2)/3$	$w = 1/[\sigma^2(F_o^2) + (0.0626P)^2]$, where $P = (F_o^2 + 2F_c^2)/3$	$w = 1/[\sigma^2(F_o^2) + (0.0P)^2 + 2.850P]$, where $P = (F_o^2 + 2F_c^2)/3$	$w = 1/[\sigma^2(F_o^2) + (0.0209P)^2 + 5.8358P]$, where $P = (F_o^2 + 2F_c^2)/3$
$(\Delta/\sigma)_{max}$	0.001	<0.0001	0.001	0.001	0.027
$\Delta\rho_{max}$, $\Delta\rho_{min}$ (e Å^{-3})	0.36, −1.18	0.74, −0.96	1.14, −1.08	0.71, −0.52	1.82, −1.85
Extinction method	None	None	None	*SHELXL*	None
Extinction coefficient	–	–	–	0.0095 (9)	–

Computer programs used: *CrysAlisCCD* (Oxford Diffraction, 2003*a*), *CrysAlisRed* (Oxford Diffraction, 2003*b*), *SHELXS*97 (Sheldrick, 1990), *SIR*-2002 (Burla *et al.*, 2003), *SHELXL*97 (Sheldrick, 1997).

(iii) $|k| = 1, 5, 7$: the reciprocal space points coming from both components are close to one another, but neither are close enough to fall into class 2 nor far enough apart to be incorporated into class 1. These reflections were removed from the reflection file because they could not be integrated properly. A similar procedure for non-merohedral twins was described by Herbst-Irmer & Sheldrick (1998). In the case of (1), this led to generally acceptable results: the R_1 value is 0.058 and the geometry, packing scheme *etc.* are reasonable.

In all cases non-H atoms were refined anisotropically, H atoms were placed geometrically and refined using the riding model, with U_{iso} set at 1.2 (1.3 for methyl group) times the U_{eq} value of the appropriate carrier atom. Only at 120 K were the H atoms refined with isotropic thermal parameters. The data

collection and structure refinement details for the best models at 295, 250, 200, 120 and 100 K are listed in Table 1.

3. Results and discussion

3.1. Continuous phase transition: 295–120 K

The structure of (1) (atom numbering in Fig. 2) at room temperature (295 K) is best described in the space group $P2_1/m$ with $Z = 2$ (*i.e.* $Z' = 1/2$). The molecule of (1) has imposed mirror symmetry: the perfectly planar nitroimidazole fragment lies on the mirror plane and the phenyl ring is perpendicular to this plane (this model will be referred to as model *A*). The refinement goes quite smoothly (R_1 converges at 0.029), but some displacement ellipsoids suggest the possibility of disorder. The ellipsoids for the C atoms of the phenyl ring are more eccentric than expected. The ratio between the largest and the smallest eigenvalue of the U^{ij} tensor (hereafter referred to as ϵ) can be interpreted as the measure of such eccentricity. In this case the values of ϵ are as large as 7.6 (C14) and 5.1 (C13).

The symmetry of the molecule might actually be lower, in which case the appropriate space group would be $P2_1$ (model B). The *R* values in this case are also acceptable ($R_1 = 0.031$), but large correlation coefficients make this refinement unstable and the results are less reliable than the s.u.'s suggest. Furthermore, the eccentricities of the U^{ij} ellipsoids are not smaller than in the $P2_1/m$ model (largest values of ϵ are 7.9 for C13 and 7.7 for C14).

There is yet another possibility (model C): the apparent symmetry of the molecule is really an artefact of the static disorder in a larger unit cell that corresponds to the space group $P2_1/c$ ($Z = 4$). This model was also checked, but the *R* factor is larger ($R_1 = 0.036$) and the ellipsoids look worse (the ϵ values are as high as 12.8 for C13 and 9.8 for C14).

It can be concluded that at room temperature the most appropriate model is A with the symmetric molecule of (1) on a special position of the $P2_1/m$ space group.

A rather similar situation is observed at 250 K. At this temperature, model A is even more favourable: its statistics are better than for the other models and the model of the thermal motion is far more physically reasonable: for model A the largest value of ϵ is 4.9, while for models B and C these values are 10.4 and 20.8. It might also be noted that models A and C are stable in the sense that (regardless of the shapes of thermal ellipsoids) the values of equivalent *U* parameters decrease consistently and by almost the same ratio: the mean values of $U_{eq}(250)/U_{eq}(295)$ are 0.87 (3) for A and 0.88 (4) for C (*cf.* Table 2). On the contrary, values of this ratio for model

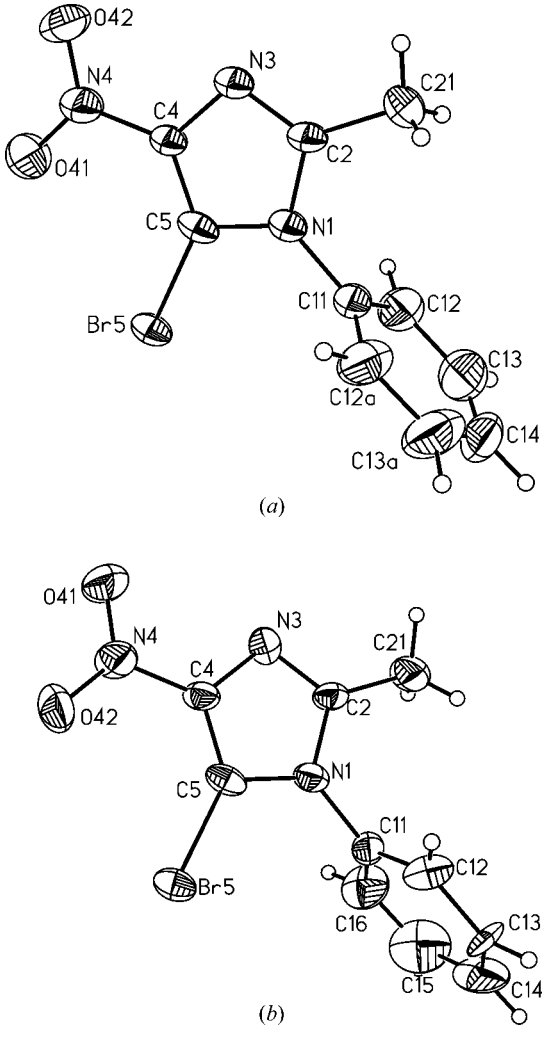

Figure 2
Anisotropic ellipsoid representation (Siemens, 1989) of molecule (1), together with the atom labelling scheme, at 250 K: (*a*) for model A ($P2_1/m$) and (*b*) for model C ($P2_1/c$). Ellipsoids are drawn at the 50% probability level; H atoms are depicted as spheres with arbitrary radii.

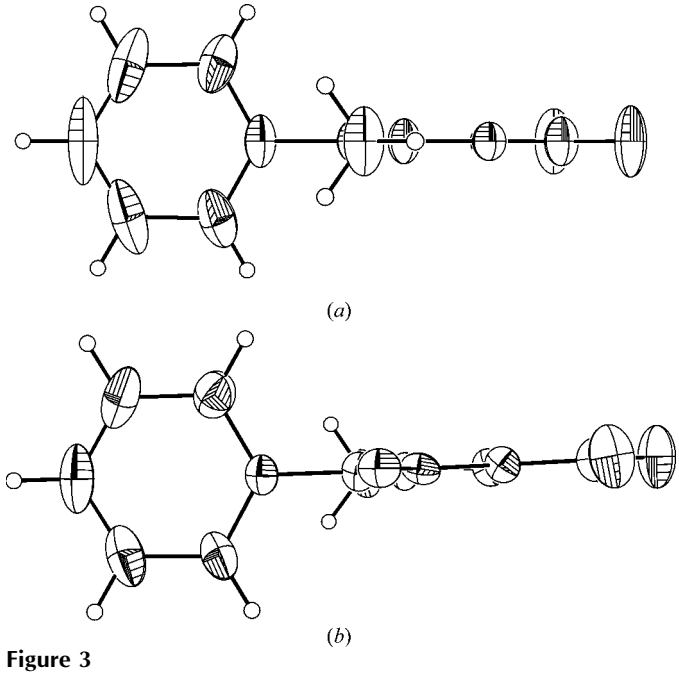

Figure 3
Anisotropic ellipsoid representation (Siemens, 1989) of molecule (1) at 200 K: (*a*) for model A ($P2_1/m$) and (*b*) for model C ($P2_1/c$). Ellipsoids are drawn at the 50% probability level; H atoms are depicted as spheres with arbitrary radii.

Table 2
Mean values of the equivalent displacement parameter ratios for the same atoms at different temperatures as compared with 295 K.

T (K)	Model		
	A ($P2_1/m$)	B ($P2_1$)	C ($P2_1/c$)
250	0.87 (3)	0.90 (9)	0.88 (4)
200	0.85 (8)	0.87 (8)	0.70 (4)
170	0.95 (22)	1.00 (25)	0.62 (4)
150	0.99 (32)	0.98 (27)	0.54 (3)
120	1.06 (48)	0.86 (41)	0.39 (2)

B are a little larger, 0.90 (9), and there are even two atoms for which the values are larger than 1.0. The large variation of the $U_{eq}(250)/U_{eq}(295)$ ratios could be regarded as additional proof of the instability of this refinement. Figs. 2(*a*) and (*b*) show the anisotropic ellipsoid representations of (1) at 250 K in model A (Fig. 2*a*) and C (Fig. 2*b*).

The results obtained at 200 K show that the descriptions in models A and C are almost equivalent. The *R*-factor values are still better for model A, but the anisotropic displacement ellipsoids are more eccentric in A (values of ϵ up to 8.9) than in C, where the maximal value of ϵ is 4.3. Also the changes in equivalent *U* parameters are still internally consistent, as can be judged from the values of e.s.d.'s of the ratios of appropriate U_{eq} values. However, it looks like more physical meaning can be attributed to model C, where the mean value of the ratio $\langle U_{eq}$ (200 K)/U_{eq} (295 K)$\rangle$ is 0.70 (4) and of $\langle U_{eq}$ (250 K)/U_{eq} (295 K)$\rangle$ is 0.79 (5). From this point of view, model A at 200 K is apparently worse than at 250 K. The appropriate ratios are 0.85 (8) and 0.97 (9) for the comparisons with 295 and 250 K. The anisotropic ellipsoid representations of (1) at 200 K are presented in Fig. 3(*a*) (model A) and (*b*) (model C).

At temperatures between 200 and 120 K, model C becomes by far the best (Fig. 4*b* presents the result at 120 K). Models A (Fig. 4*a*, also at 120 K) and *B* – even though they still allow for structure solution and successful refinement and give geometrical parameters that are reasonable – are increasingly unsatisfactory in terms of anisotropic displacement parameters. The values of ϵ are as large as 55 and the behaviour of the equivalent *U* value is strange. Table 2 lists the values of $\langle U_{eq}(T)/U_{eq}(295)\rangle$ for different models. For model C, and only for this model, the mean changes of U_{eq} correlate well with the temperature; the *R* value is 0.994. It might be noted that the atoms in the imidazole ring behave quite properly; the strange behaviour is confined to the substituents (Figs. 4 and 5).

Another insight into the nature of the ongoing phase transition might be gained by the analysis of the reflection intensities at different temperatures. The presence of a flat molecule close to $y = 0.25$ and approximately parallel to the (010) plane in the space group $P2_1/c$ should result in a systematic weakening of the reflections with odd *l* indices. The limiting case is the exact symmetry, when all reflections that have odd *l* indices are systematically absent and therefore the appropriate unit cell is smaller: $c' = c/2$ and the space group is $P2_1/m$ with $Z = 2$.

Therefore, the diffraction data were analysed at each temperature in the larger unit cell (as in model C) and the intensities of reflections with *l* even and odd were compared.

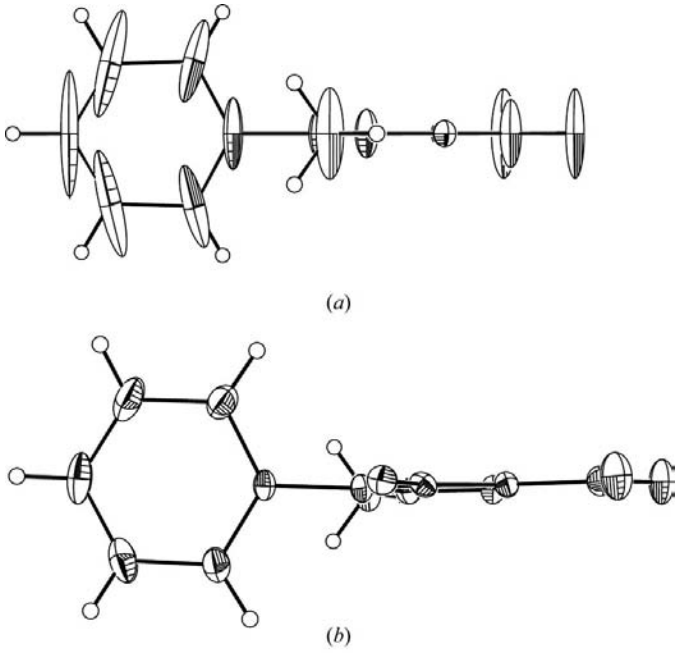

Figure 4
Anisotropic ellipsoid representation (Siemens, 1989) of molecule (1) at 120 K: (*a*) for model A ($P2_1/m$) and (*b*) for model C ($P2_1/c$). The ellipsoids are drawn at the 50% probability level; H atoms are depicted as spheres with arbitrary radii.

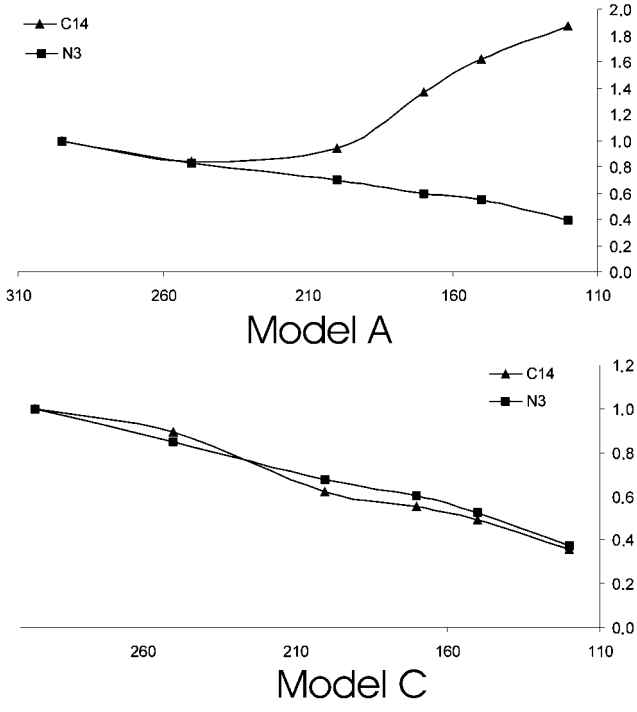

Figure 5
The changes of the ratio $U_{eq}(T)/U_{eq}(295)$ as a function of temperature for two atoms: C14 (from the phenyl ring) and N3 (from the imidazole ring) for different models.

Table 3
Selected geometrical parameters (Å, °) with s.u.'s in parentheses.

	T (space group)				
	295 ($P2_1/m$)	250 ($P2_1/m$)	200 ($P2_1/c$)	120 ($P2_1/c$)	100 ($P\bar{1}$)
N1—C2	1.381 (3)	1.365 (6)	1.373 (5)	1.382 (3)	1.375 (9)
N1—C5	1.380 (3)	1.382 (6)	1.371 (5)	1.369 (3)	1.361 (9)
N1—C11	1.438 (4)	1.452 (6)	1.450 (5)	1.444 (3)	1.442 (10)
C2—N3	1.303 (4)	1.320 (6)	1.319 (5)	1.313 (3)	1.311 (10)
N3—C4	1.374 (4)	1.364 (6)	1.369 (6)	1.366 (3)	1.363 (9)
C4—N4	1.421 (4)	1.430 (6)	1.426 (6)	1.424 (3)	1.432 (10)
N4—O41	1.220 (4)	1.225 (5)	1.221 (5)	1.230 (3)	1.229 (8)
N4—O42	1.225 (4)	1.221 (5)	1.229 (5)	1.233 (3)	1.228 (8)
C5—Br5	1.855 (2)	1.853 (4)	1.851 (4)	1.850 (2)	1.857 (7)
C5—N1—C2	107.3 (2)	108.1 (4)	108.3 (3)	107.9 (2)	107.7 (6)
N1—C2—N3	111.5 (2)	111.2 (4)	111.0 (4)	111.1 (2)	111.5 (6)
C2—N3—C4	105.1 (2)	104.4 (4)	104.5 (3)	105.1 (2)	104.8 (6)
N3—C4—C5	111.9 (3)	112.9 (4)	112.5 (4)	112.0 (2)	111.7 (6)
C4—C5—N1	104.2 (2)	103.3 (4)	103.6 (3)	103.9 (2)	104.2 (6)
C4—C5—Br5	135.2 (2)	136.3 (4)	135.7 (3)	135.3 (2)	134.9 (6)
N1—C5—Br5	120.6 (2)	120.4 (3)	120.6 (3)	120.8 (2)	120.7 (5)
|C5—N1—C11—C12|	90.5 (2)	91.3 (4)	92.2 (6)	95.2 (3)	91.5 (11)
Ph/Im	90	90	88.85 (18)	87.02 (11)	86.9 (3)
Im/NO_2	0	0	1.38 (15)	0.60 (13)	2.7 (5)

The results are fully consistent with the previous analysis. At room temperature, the ratio of $\langle I/\sigma(I)\rangle_{l\ \mathrm{even}}$ and $\langle I/\sigma(I)\rangle_{l\ \mathrm{odd}}$ is 20.1, and this ratio decreases systematically on lowering the temperature (Fig. 6). Since the molecules of (1) are still close to the plane parallel to (010) at y = 1/4 – the possibility of successful refinement of the models A and B proves this – the reflections with l odd are weaker than those with l even; the changes in the ratio of $\langle I/\sigma\rangle$ indicates the growing discrepancies from the exact C_s symmetry. Fig. 7 shows the comparison of two frames taken at the same diffractometer angles: there are additional reflections with l odd in the picture at 150 K.

This phase transition is of an order–disorder nature and because it continues over a temperature range it should be classified as a second-order transition. Such a transformation may be described by the decrease of an order parameter with rising temperature (Herbstein, 1996). A convenient order parameter in the present case could be the intensity of the reflections with l-odd indices. Since the data collections were performed for different crystals and with different strategies, the most useful parameter turned out to be the ratio of sums of intensities for l odd and for all reflections, $\sum I_{hkl}(l = 2n + 1)/\sum I_{hkl}$(all) [a similar dependence was discussed for example by Katrusiak (2000) in the studies of the order–disorder phase transition in 2-methyl-1,3-cyclohexanedione crystals]. The plot of this ratio for T < 250 K is shown in Fig. 8. This function suggests that the critical temperature lies around 220 K, in accordance with the behaviour of the unit-cell constants. This value of the critical temperature is, however, an approximation only – even at higher temperatures there are reflections with l odd of significant intensity. On the basis of structure refinements and structural data it might be stated that at 250 K the structure is in the α-phase and at 170 K in the β-phase, but between these temperatures the choice of a proper phase is a matter of taste rather than solid fact. A similar situation was explained by Xia *et al.* (2001) by the coexistence of regions of both phases at some temperatures.

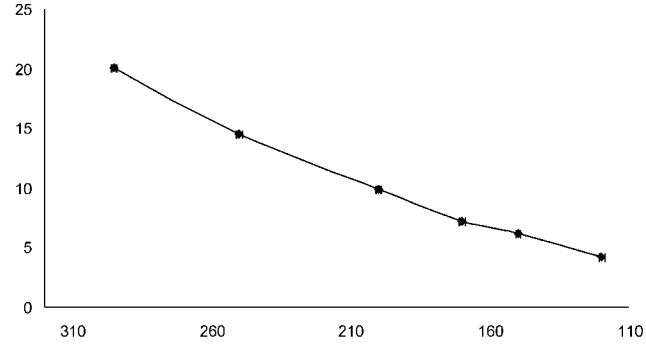

Figure 6
The $\langle I/\sigma(I)\rangle_{\mathrm{even}}$ and $\langle I/\sigma(I)\rangle_{\mathrm{odd}}$ ratio for model C (large unit cell) as a function of temperature (r = 0.992).

3.2. Phase transition and twinning (115 K)

When the temperature is lowered below 120 K the sample undergoes another phase transition that is also reversible. The structure becomes triclinic, space group $P\bar{1}$, but at the same time the crystal undergoes twinning. Fig. 9 shows the changes in the diffraction pattern when the temperature drops from 120 to 100 K.

The result of this transition is shown in Fig. 1, which shows the reciprocal space representation of the strongest reflections from the whole measurement. Two alternative unit-cell orientations, related by a mirror plane can be found in this picture. Refinement was conducted according to these observations (*cf.* §2).

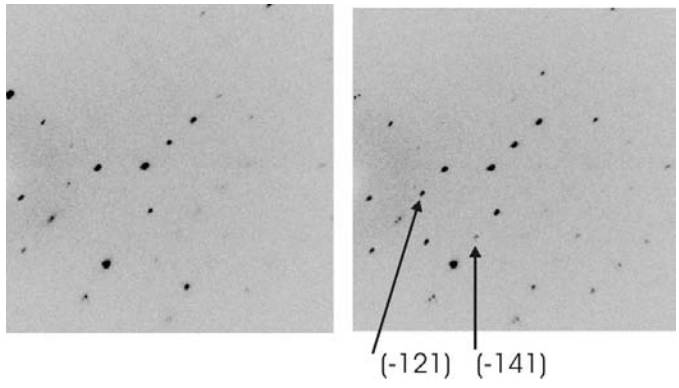

Figure 7
Diffraction images taken with the same crystal orientation at different temperatures: (left): 250 K and (right) 150 K. The reflections with l odd indices appear at lower temperatures; two of them are marked with arrows and indexed.

Table 4
Intermolecular interaction data: halogen bonds, dihalogen bonds and weak C—H···Br hydrogen bonds.

	T (space group)				
	295 K($P2_1/m$)	250 K ($P2_1/m$)	200 K ($P2_1/c$)	120 K ($P2_1/c$)	100 K ($P\bar{1}$)
N3···Br5^{i}	2.952 (2)	2.940 (4)	2.917 (3)	2.895 (2)	2.886 (6)
C2—N3···Br5^{i}	115.3 (2)	115.8 (3)	115.6 (2)	115.07 (14)	115.0 (4)
C4—N3···Br5^{i}	139.5 (2)	139.8 (3)	139.9 (3)	139.85 (15)	140.2 (5)
N3···Br5^{i}—C5^{i}	162.88 (10)	163.2 (2)	163.07 (15)	163.13 (8)	163.4 (2)
Br5···Br5^{ii}	3.5990 (5)	3.5920 (6)	3.5545 (9)	3.5190 (6)	3.5195 (14)
Br5···Br5^{iii}	3.5990 (5)	3.5920 (6)	3.5855 (9)	3.5767 (6)	3.5669 (14)
C5—Br5···Br5^{ii}	75.66 (1)	75.33 (2)	75.87 (13)	76.02 (8)	75.8 (2)
C5—Br5···Br5^{iii}	75.66 (1)	75.33 (2)	74.37 (13)	73.96 (8)	74.6 (2)
H21*B*···Br5^{i}	2.98	2.97	2.96	3.01 (4)	2.98
C21···Br5^{i}	3.746 (4)	3.753 (7)	3.735 (5)	3.707 (3)	3.697 (8)
C21—H21*B*···Br5^{i}	137	138	137	138 (3)	131

Symmetry codes: for the α-phase: (i) $-1+x, y, z$; (ii) $2-x, -y, 1-z$; (iii) $2-x, -y, 1-z$; for the β-phase: (i) $1+x, y, z$; (ii) $1-x, 1-y, 1-z$; (iii) $1-x, -y, 1-z$; for the γ-phase: (i) $-1+x, y, z$; (ii) $-x, 1-y, -z$; (iii) $-x, 2-y, -z$.

The phase-transition-induced twinning is observed relatively frequently for inorganic structures, but such a phenomenon has also been described in some non-inorganic compounds, for example, over 40 years ago in 1,2,4,5-tetrabromobenzene (Gafner & Herbstein, 1960) and, more recently, in 2,6-dimethylpyridine *N*-oxide semiperchlorate (Jaskólski *et al.*, 1978), triferrocenylboroxine and triferrocenylborazine (Bats *et al.*, 2002), *trans*-tetraaquabis(trifluoroacetato-*O*)manganese(II) (Olejnik & Lis, 2000) and the 1:1 adduct of hexamethylenetetramine and azelaic acid (Hostettler *et al.*, 1999).

3.3. Unit-cell parameters

Fig. 10 shows the changes of the unit-cell parameters with temperature. The data for different points were determined for two different crystals (*cf.* §2) and generally they fit the same temperature dependence.

For the 200–120 K range the *c*/2 parameter of the space group $P2_1/c$ (model C) is drawn (this parameter is also used for the calculation of unit-cell volume). A small abnormality is observed near 220–190 K. Further analysis (see above), especially of the displacement ellipsoids, testify for the presence of this subtle effect. There is also a drop in the $V(T)$ function between 120 and 115 K (Fig. 10*b*) that is in accordance with the first-order character of the phase transition (Herbstein, 1996).

It might be noted that for model C (Z' = 1) the reduced cell corresponds to the $P2_1/n$ space group (for example, at 170 K, c = 22.067 Å, $\beta = 91.29^\circ$); the $P2_1/c$ setting was chosen because it is related in a simpler way to the *reduced* unit cell of the models A and B ($100/010/00\frac{1}{2}$). Also, the unit-cell setting of the low-temperature triclinic phase (the standard unit cell is: a = 6.823, b = 6.971, c = 11.402 Å, α = 106.52, β = 92.69, $\gamma = 90.31^\circ$) was chosen in order to keep the correspondence with the high-temperature phases.

The temperature dependence of the unit-cell parameters is in agreement with the observation, on the basis of structural analyses, that there are two phase transitions in the studied range: the first one around 200 K and of second order, and the second one between 120 and 110 K and probably of first order.

3.4. Molecular structure

The selected bond lengths and angles are listed in Table 3. There is a noticeable effect of the nitro substituent on the intraannular ring angles, similar to that described by Domenicano & Murray-Rust (1979) for phenyl derivatives. The N3—C4—C5 angle in (1) is (on average) 2.5° larger than in unsubstituted imidazole (McMullan *et al.*, 1979), while the two adjacent intraannular angles are smaller. The exocyclic angles at C5 show the characteristic asymmetry (Table 3) caused by steric repulsion between the Br atom and the nitro group, which is almost coplanar (or perfectly coplanar) with the imidazole ring. The steric repulsion between the Br atom and

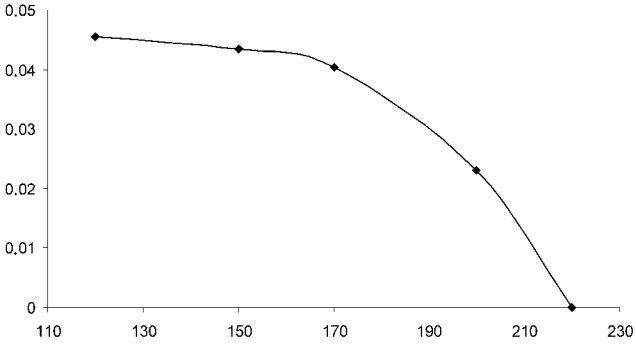

Figure 8
Plot of the temperature dependence of the ΣI_{hkl} (l odd)/ΣI_{hkl} (all) ratio for $T < 250$ K. The last point on the right is added by extrapolation of the curve.

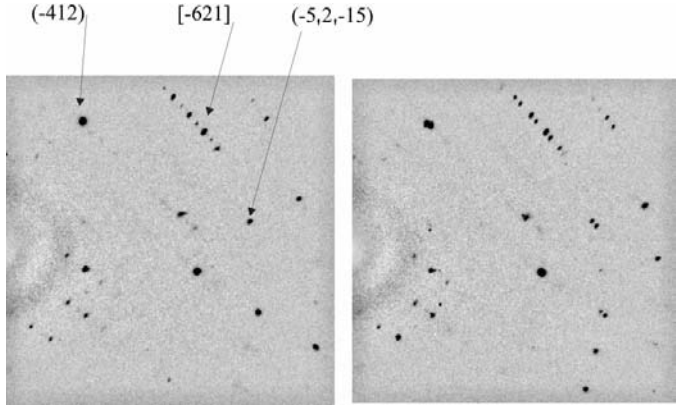

Figure 9
Diffraction images taken at the same crystal orientation at different temperatures: (left): 120 K and (right) 100 K. The results of twinning can be seen *e.g.* in the [−62*l*] line and in the splitting of some reflections.

the phenyl ring H atoms is also probably the reason for the large dihedral angle between the phenyl and imidazole rings (Table 3).

There are no significant differences in bond lengths and angles that could not be attributed to the change of temperature and/or to the twinning in the γ-phase. The only significant and decisive change can be observed in the conformation of the molecule. In the α-phase, owing to the symmetry requirements, the imidazole ring is perfectly planar, the C (methyl), Br and NO_2 substituents are exactly coplanar with the ring, and the phenyl ring is perpendicular to the ring. As the temperature decreases the deviations from this model are more and more important, and can no longer be reasonably described by the displacement ellipsoids. At 200 K model C (β-phase) starts to be a better description, the imidazole ring is not ideally planar (although it is still planar to a good approximation, with maximal deviations from the least-squares plane no larger than 3σ) and the angle between this ring and the phenyl ring differs from the ideal exact value of 90° observed in the α-phase (Table 2, Fig. 11). The deviations are not very impressive, but still large enough to break the symmetry.

3.5. Crystal packing

Fig. 11 shows a comparison of the crystal packing at three different temperatures and for three different phases. Obviously these packing modes are almost identical; there are no sharp changes in the intermolecular interactions when the crystal undergoes the phase transitions. The absence of major changes might be one of the reasons for the reversibility of these transitions.

Two main factors that determine crystal packing are the C—Br···Nr halogen bonds and dihalogen Br···Br interactions.

The intermolecular N···Br—C interactions connect the molecules of (1) (regardless of phase) into infinite chains along the [100] direction (Fig. 12). These chains are additionally strengthened by weak C—H···Br interactions. For the contacts C(heterocycle)—Br···N(heterocycle) the Br···N distances in (1) (Table 4) are the shortest contacts of this kind

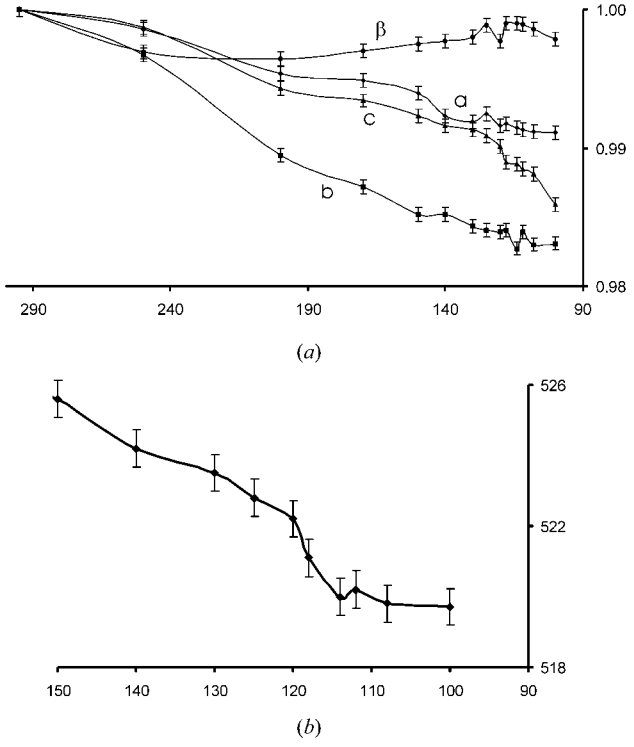

Figure 10
Plot of changes in (*a*) the unit-cell parameters as a function of temperature in the range 295–100 K and (*b*) the unit-cell volume as a function of temperature in the range 150–100 K.

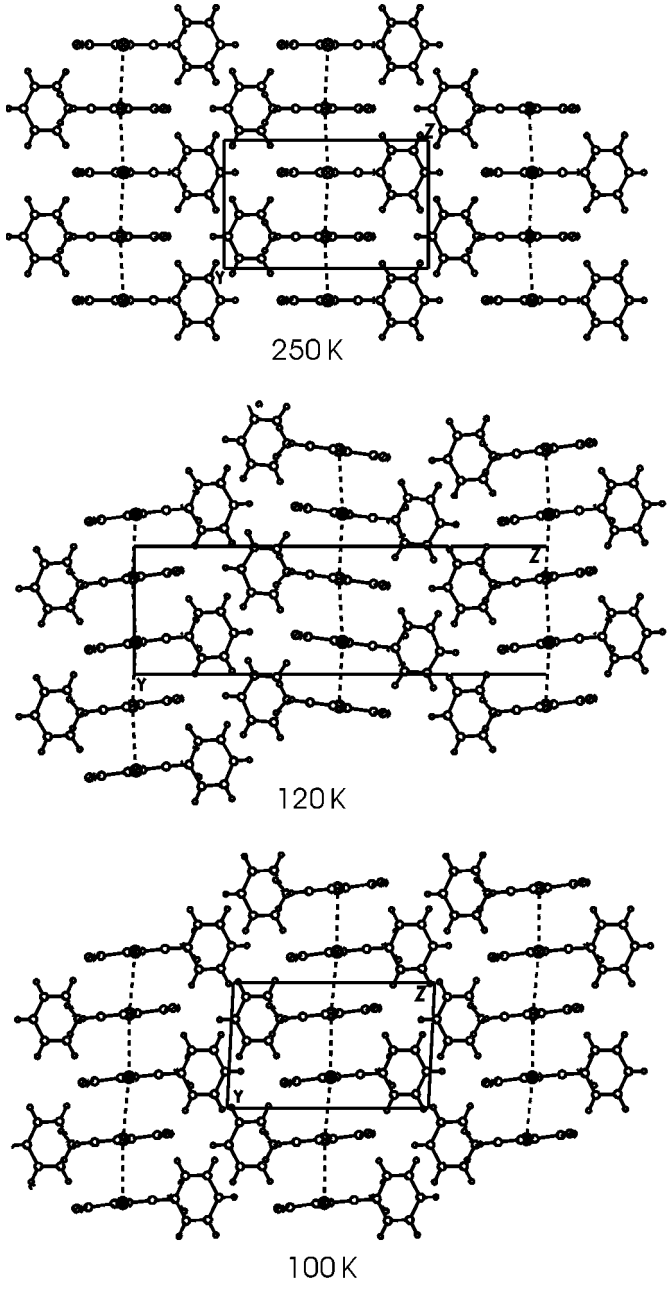

Figure 11
The packing schemes at different temperatures as seen along [100]. Dashed lines depict Br···Br interactions.

found so far. A CCDC survey (Allen, 2002) shows that shorter contacts can be found only for complexes with CBr_4. The geometry of these halogen bonds is typical, almost linear C—Br···N angles testify for the proposed mechanism of this interaction (see §1). The attack of Br is close to the direction of the nitrogen lone pair. The C—Br group is coplanar (or almost coplanar) with the imidazole plane of a neighbouring molecule – the halogen bonds therefore help to form the molecular tapes.

The other chains of molecules are made by means of Br···Br interactions along the [010] direction. These interactions are of type I according to the classification of Ramasubbu *et al.* (1986): the two C—Br···Br angles are equal (owing to the symmetry requirements, in every phase the molecules connected by Br···Br interactions are related by a centre of symmetry). In the symmetrical α-phase two Br···Br distances are equal and with the loss of symmetry they become different (Table 4).

There are, if any, only very weak intermolecular C—H···O interactions with the nitro group O atoms; also there are no nitro···nitro interactions (Woźniak *et al.*, 2002). In similar nitroimidazole derivatives weak C—H···N and C—H···O hydrogen bonds determine the crystal packing. The imidazole N3 atom does not take part in any interactions other than Br···N interactions. These observations prove that halogen bonding can successfully compete with weak hydrogen bonds and act as the primary driving force in the crystal packing determination, *i.e.* in creating a supramolecular assembly.

4. Conclusions

The crystal structure of (1) undergoes two phase transitions between room temperature and 100 K. The first, around 200 K, is a second-order, continuous phase transition of an order–disorder nature, without a change in Laue group. The space group changes from $P2_1/m$ (α-phase, above 220 K) to $P2_1/c$ (β-phase) and the c parameter of the unit cell doubles. During this transition the molecule loses the exact C_s symmetry observed in the room-temperature α-phase. The second transition, around 115 K, is connected with a change of point group (the γ-phase, below 115 K, crystallizes in the triclinic $P\bar{1}$ space group) and with twinning. The crystal packing, which is mainly governed by halogen C—Br···N and dihalogen Br···Br bonds, does not change substantially during these transitions. The former are among the shortest interactions of this type found; the latter are of the non-specific type I, according to the classification of Ramasubbu *et al.* (1986).

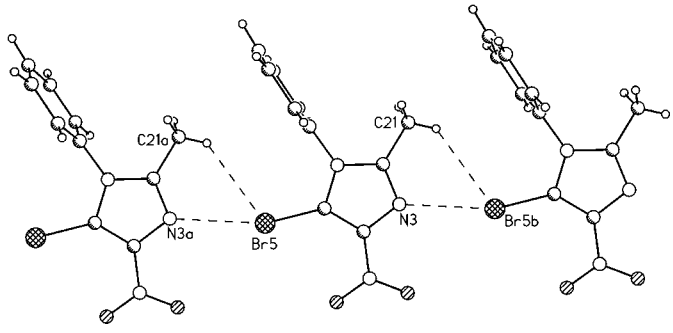

Figure 12
Main halogen-bond motif in the crystal structure of (1), as seen approximately along the [010] direction. Halogen C—Br···N bonds and weak hydrogen C—H···Br bonds are depicted as dashed lines. Symmetry codes: (*a*) $-1+x, y, z$; (*b*) $1+x, y, z$.

The author wishes to thank Dr Paweł Wagner for providing the compound and for stimulating discussions. The thoughtful remarks of the referees and the Editor helped significantly in the final shaping of this paper.

References

Allen, F. H. (2002). *Acta Cryst.* B**58**, 380–388.
Bats, J. W., Ma, K. & Wagner, M. (2002). *Acta Cryst.* C**58**, m129–m132.
Bent, H. A. (1968). *Chem. Rev.* **68**, 587–648.
Blessing, R. H. (1989). *J. Appl. Cryst.* **22**, 396–397.
Burla, M. C., Camalli, M., Carrozzini, B., Cascarano, G. L., Giacovazzo, C., Polidori, G. & Spagna, R. (2003). *J. Appl. Cryst.* **36**, 1103.
Dahl, T. & Hassel, O. (1970). *Acta Chem. Scand.* **24**, 377–382.
Dahl, T. & Hassel, O. (1971). *Acta Chem. Scand.* **25**, 21682174.
Domenicano, A. & Murray-Rust, P. (1979). *Tetrahedron Lett.* **24**, 2283–2286.
Gafner, G. & Herbstein, F. H. (1960). *Acta Cryst.* **13**, 706–716.
Hassel, O. (1970). *Science*, **170**, 497–502.
Hassel, O. & Rømming, C. (1962). *Q. Rev. Chem. Soc.* **16**, 1–13.
Herbst-Irmer, R. & Sheldrick, G. M. (1998). *Acta Cryst.* B**54**, 443–449.
Herbstein, F. (1996). *Cryst. Rev.* **5**, 181–226.
Hostettler, M., Birkedal, H., Gardon, M., Chapuis, G., Schwarzenbach, D. & Bonin, M. (1999). *Acta Cryst.* B**55**, 448–458.
Jaskólski, M., Gdaniec, M., Kosturkiewicz, Z. & Szafran, M. (1978). *Pol. J. Chem.* **52**, 2399–2403.
Katrusiak, A. (2000). *Acta Cryst.* B**56**, 872–881.
Kowalski, A. (1995). *Acta Cryst.* C**51**, 1670–1672.
Kubicki, M. (2004). In preparation.
Kubicki, M., Borowiak, T., Dutkiewicz, G., Souhassou, M., Jelsch, C. & Lecomte, C. (2002). *J. Phys. Chem. B*, **106**, 3706–3714.
Kubicki, M., Borowiak, T., Suwiński, J. & Wagner, P. (2001). *Acta Cryst.* C**57**, 106–108.
Legon, A. C. (1999). *Angew. Chem. Int. Ed.* **38**, 2687–2714.
Metrangolo, P., Pilat, T., Resnati, G. & Stevenazzi, A. (2003). *Curr. Opin. Colloid Interface Sci.* **8**, 215–222.
Metrangolo, P. & Resnati, G. (2001). *Chem. Eur. J.* **7**, 2511–2519.
McMullan, R. K., Epstein, J., Ruble, J. R. & Craven, B. M. (1979). *Acta Cryst.* B**35**, 688–691.
Olejnik, Z. & Lis, T. (2000). *Acta Cryst.* C**56**, 1310–1311.
Oxford Diffraction (2003*a*). *CrysAlisCCD User's Guide*, Version 171. Wrocław, Poland: Oxford Diffraction.
Oxford Diffraction (2003*b*). *CrysAlisRed*, Version 171. Wrocław, Poland: Oxford Diffraction.
Ramasubbu, N., Parthasarathy, R. & Murray-Rust, P. (1986). *J. Am. Chem. Soc.* **108**, 4308–4314.
Rossmann, M. G. & Lipscomb, W. N. (1958). *Tetrahedron*, **9**, 275–293.
Sakurai, T., Sundaralingam, M. & Jeffrey, G. A. (1963). *Acta Cryst.* **16**, 354–363.

Sheldrick, G. M. (1990). *Acta Cryst.* A**46**, 467–473.
Sheldrick, G. M. (1997). *SHELXL*97. University of Göttingen, Germany.
Siemens (1989). *Stereochemical Workstation Operation Manual*. Release 3.4. Siemens Analytical X-ray Instruments Inc., Madison, Wisconsin, USA.
Woźniak, K., Mallinson, P. R., Wilson, C. C., Hovestreyd, E. & Grech, E. (2002). *J. Phys. Chem. A*, **106**, 6897–6703.
Wunderlich, J. A. & Lipscomb, W. N. (1960). *Tetrahedron*, **11**, 219–225.
Xia, A., Selegue, J. P., Carrillo, A., Patrick, B. O., Parkin, S. & Brock, C. P. (2001). *Acta Cryst.* B**57**, 507–516.